

Effect of Substitution of Titanium by Tin on Properties of Fe_2TiO_5

Dr. Sandesh S. Gurav*

Department of Physics, K. E. S. Anandibai Pradhan Science College, Nagothane, Maharashtra

Abstract – In order to study the properties of the tin substituted Fe_2TiO_5 based materials the samples are prepared by standard ceramic technique. The single-phase formation of the pseudobrookite is confirmed by XRD technique.

It is interesting to note that substitution of Ti^{4+} by Sn^{4+} is responsible to increase the unit cell volume and X-Ray or theoretical density. On the other hand, the use of anatase in the reaction causes the decrease in practical density and the increase in the porosity, Debye particle size and the inhomogeneity. The presence of Sn^{4+} increases the contribution towards both the space charge as well as dipolar polarization. However, the increase in the space charge is significant.

It is also interesting to note that the tin substituted samples exhibit antihystereses and $E_{a3} < E_{a2}$ for these samples. Hence these antihystereses are due to tunneling effect.

Key words: Substitution, Pseudobrookite, Antihysteresis, Tunneling effect.

-----X-----

1. INTRODUCTION:

Iron titanate is a pseudobrookite which exhibits many interesting properties such as spin glass behaviour, thermal microcracking, high resistivity, etc. A cluster approach may be used for a description of spin glass behaviour of the pseudobrookites [1]. D. A. Kharmov, et.al [1] have studied the spin glass transition in the $\text{Fe}_2\text{Ti}_{1-x}\text{Sn}_x\text{O}_5$ pseudobrookite and found that Sn^{4+} ions appear to occupy only M1/4c octahedral sites and spin glass transition temperature T_g depends on tin concentration monotonically. According to the XRD analysis and Sn-Mossbauer Spectral (MS) data the maximum solubility of Sn^{4+} ions in the pseudobrookite structure at 1250°C is $x = 0.22$ [1], where the unit cell volume increases linearly with the increasing tin concentration.

The XRD analysis of the limit of solid solution $\text{Fe}_2\text{Ti}_{1-x}\text{Sn}_x\text{O}_5$ ($0 < x < 0.25$) has been conducted by S. S. Meshalkin et al. [2] and has obtained $x = 0.18$ as the limit. A spin relaxation model has been used by G. M. Irwin et al. [3] to interpret the Fe-Mossbauer Spectral data of $(\text{Ba Sn}_x\text{Ti}_{2-x}\text{Fe}_4\text{O}_{11})$ ferric oxide spin glass. It has been suggested that, Ti-rich supermagnetic clusters (and the effect of Sn to breakup these clusters) are important in understanding the magnetic properties of this material. The model used here has been proposed to analyze the other oxide spin glasses such as Fe_2TiO_5 [3].

However, the data of electrical transport and dielectric properties of the tin containing pseudobrookite is scarce [4]. Hence it is felt necessary to investigate the electrical and dielectric properties of tin containing pseudobrookites. The following few paragraphs are devoted to the behaviour of Sn^{4+} and Sn^{4+} in the vicinity of Ti^{4+} to highlight the importance of the Sn^{4+} substitution.

SnO_2 (sintered ceramics and also compressed powder under very high pressure) exhibits an astonishingly high value of dielectric constant of the order of 10^5 [5]. Unlike other oxide semiconductors such as Ni-Zn ferrites etc. the dielectric constant of SnO_2 is not markedly dependent on the applied frequency in the audio frequency range. However, in the R. F. range the dielectric constant decreases with frequency [5]. A dielectric hysteresis loop has been observed in SnO_2 [5].

The influence of a small amount of SnO_2 on the structural changes of nano-crystalline TiO_2 has been investigated [6]. It is observed that small amount of SnO_2 doping enhances the rutilation of anatase and effectively prohibits the grain growth in these powders [6]. The incorporation of about 17% of Sn completely transforms anatase to the rutile form at a calcination temperature as low as 500°C [7]. The optical analysis shows that the band gap and Fermi level of the $\text{Ti}_{1-x}\text{Sn}_x\text{O}_2$ solid solutions increases with increasing x and these solid solutions are expected to be of better photocatalytic properties [7]. The

electrical measurements on ohmically metal electroded sintered pellets of Ti_x Sn_{1-x} O₂ (0 < x < 0.25) system with small amounts of dopants such as Al, Co, Nb have shown the nonlinear I-V characteristics [8]. The nonlinear coefficient is found to decrease with increase in x. On the other hand breakdown voltage (Eb) shows the increase with the increase in x. The low current in the pre breakdown region implies that the grain boundary resistance is high for the solid solutions. However, the grain boundary barrier or energy barrier is ineffective. The solubility of Ti⁴⁺ ions in SnO₂ is up to 25 mole %.

SnO₂ has been supported on TiO₂, Al₂O₃, MgO and SiO₂ [9]. The reduction of the species is easier if it is present on the surface than within the structure of support. It is found that on titania a smaller Quadrupole Splitting (QS) is observed, which might be explained assuming that Sn⁴⁺ is inside the structure of the titania. This is in agreement with the findings reported by Bartholomew and Boudart [10], who have reported that the Quadrupole Splitting (QS) for an atom in a crystal is lower than on the surface.

Ceramic bodies have been prepared from the ferric stannates and their dielectric properties have been measured [11]. They are found to be semiconductor. The resistivity of Fe₂(SnO₃)₃ as determined using the direct current at room temperature is 10⁴ Ω-cm. The addition of this stannate to BaTiO₃, may be effective in decreasing maturing temperature and improving body density. The substitution of Sn⁴⁺ ion for the Ti⁴⁺ ion may also be expected to improve the stability of titanate bodies with regard to changes in the state of oxidation during normal firing treatment, since SnO₂ is more stable in this respect than TiO₂ [12]. The Mossbauer Spectral (MS) data of tin doped Fe₃O₄ recorded at elevated temperature in vacuum shows the decrease in the Curie temperature with increase in concentration of the dopant [12]. The MS data recorded from all tin doped iron oxides show the presence of a hyperfine magnetic field at the Sn⁴⁺ sites. The study of Reitveld structure refinement of XRD of tin doped α-Fe₂O₃ has been reported to contain tin in both interstitial and substitutional sites of the corundum-related α-Fe₂O₃ structure [13]. Zirconium titanate-stannate solid solutions Zr_{1-x} Sn_x TiO₄ are known to have a high dielectric constant, a high Q-value and a low temperature coefficient of resonant frequency [14].

2. RESULTS AND DISCUSSION:

2.1 STRUCTURAL PROPERTIES:

The structural properties of the samples namely Fe₂TiO₅ using rutile TiO₂ [FTR], Fe₂TiO₅ using anatase TiO₂ [FTA], Fe₂Ti_{0.75}Sn_{0.25}O₅ using rutile TiO₂ [FTSR] and Fe₂Ti_{0.75}Sn_{0.25}O₅ using anatase TiO₂ [FTSA] all synthesized at 1250°C are reported here. The data is indexed in a single phase orthorhombic structure having the space group Bbmm of the pseudobrookite. Hence it is concluded

that all the samples [FTR], [FTA], [FTSR] and [FTSA] are pseudobrookites. In the present work the systematic investigation of these properties of pseudobrookites [FTSA] and [FTSR] prepared from anatase and rutile phases of TiO₂ and sintered at 1250°C is made and their properties are compared with those of pure samples [FTA] and [FTR] respectively.

2.2 Dielectric Properties:

For a given ceramic, the dielectric constant (K') depends on the factors such as electron polarization, atomic polarization, interfacial polarization (space charge) and dipolar polarization at micro level [4]. Also it is known to depend on the parameters such as particle size, porosity, inter-granular phases, lattice impurities on the grain boundaries, sintering temperature, etc. at macro level [4,16]. Therefore dielectric constants of our samples at room temperature at 1kHz, 10 kHz, 100 kHz, 1000 kHz, Debye particle size, porosity, inhomogeneity and space charge (defined as K'_{1kHz}·K'_{1000 kHz}) are included in the Table-1 to facilitate the comparison.

Table-1: Data showing Dielectric Constant (K') at 1 kHz, 10 kHz, 100 kHz, 1000 kHz at Room Temperature.

Sample	K' _{1kHz}	K' _{10kHz}	K' _{100kHz}	K' _{1000kHz}	Debye particle size (Å)	Porosity	Inhomogeneity	Space charge K' _{1000kHz} /K' _{1kHz}	Order Parameter δ'	Loop Area of K' hysteresis (Wb/m ²)
FTR	3407	1404	329	75.0	540	0.008	-0.0020	3.021	0.310	3.02
FTA	1130	1117	794	329	634	0.14	-0.0038	7.91	0.040	4.00
FTSR	3028	1516	567	123	450	0.033	-0.0025	3.705	3.000	2.75
FTSA	3603	2650	2300	460	652	0.23	-0.0030	3.203	0.060	6.30

It is observed that the anatase causes the reduction in the space charge. If K'_{1000 kHz} represents the contribution to the dipolar polarization, then interestingly the anatase enhances the dipolar polarization considerably.

On the other hand, the presence of Sn⁴⁺ increases the contribution towards both the space charge as well as dipolar polarization. However, the increase in the space charge is significant. The space charge appears to have a weak inverse dependence on the inhomogeneity, porosity, and the Debye particle size. On the other hand, the dipolar contribution (K'_{1000 kHz}) has a weak direct dependence on these structural parameters.

2.2.1 Relaxation Spectra:

In order to obtain more information about the space charge the relaxation spectra of the samples are also investigated. The plots (i) K' v/s log (frequency) and (ii) K'' v/s log (frequency) and (iii) tan (δ) Vs log (frequency), known as relaxation spectra of the samples are given in Figures-1 to 3 respectively. The nature of the curves is similar to that shown by Maxwell-Wagner model for the space charge. The shapes of the curves indicate the presence of the space charge in all the four samples. (K'_{1kHz} - K'₁₀₀₀)

kHz) which is taken as measure of the space charge, is maximum in sample [FTSR].

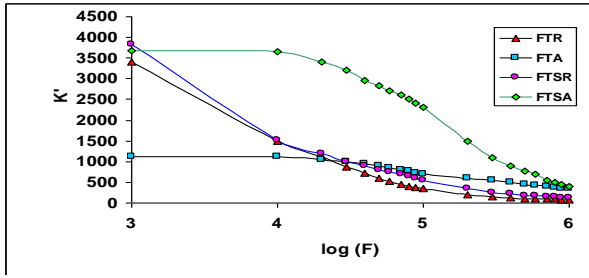


Figure-1 Plot of Dielectric Constant (K') Vs log(F)

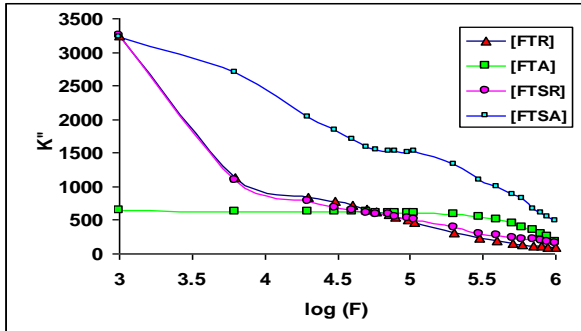


Figure-2 Plot of Dielectric loss (K'') Vs log(F)

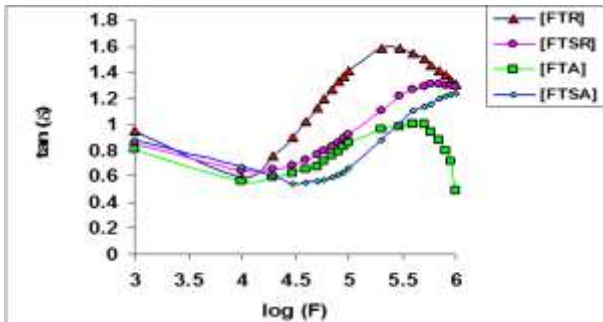


Figure-3 Plot of tan (δ) Vs log(F)

2.2.2 Variation of Dielectric Constant (K') with Temperature:

The variation of dielectric constant K' with temperature (300-650 K) is investigated for all the samples. The variation of dielectric constant K' with temperature for [FTR], [FTSR], [FTA] and [FTSA] are shown in the Figures-4 to 7 respectively. The dielectric constant K' first increases slowly to saturate approximately above temperature 600 K. The heating and cooling cycles exhibit distinct hysteresis curves. The hysteresis curves in the Figures-4 and 5 are measured for the samples [FTR] and [FTSR] respectively at 1 kHz and therefore correspond mainly to the space charge. [FTSR] exhibits antihysteresis. Whereas, the hysteresis curves in the Figures-6 and 7 are measured for the samples [FTA] and [FTSA] respectively at 1000 kHz and therefore correspond also to the dipolar contribution. This is because the samples prepared from rutile

phase of TiO_2 show very narrow hysteresis curves even at 1 kHz.

It is interesting to note that the presence of space charge (which takes part in electrical conduction) means the loops correspond to the thermal diffusivity [17]. In [FTSA] a square loop super imposed on the thermal diffusivity corresponds to the dipolar component.

Overall, the loop area is increased by the anatase and Sn^{4+} has opposite effects on the rutile and anatase. The loop area is better described in terms of the order parameter λ' which depends on the cation distribution. The hysteresis of space charge decreases in area whereas hysteresis of dipolar polarization increases in area with the increase in order parameter λ' .

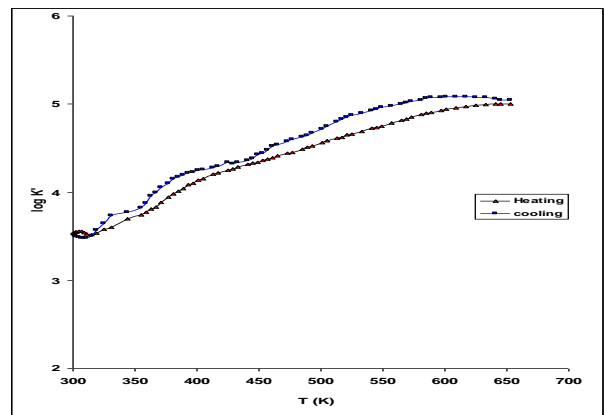


Figure-4. Plot of Dielectric Constant ($\log K'$) Vs temperature(T) for the sample[FTR]

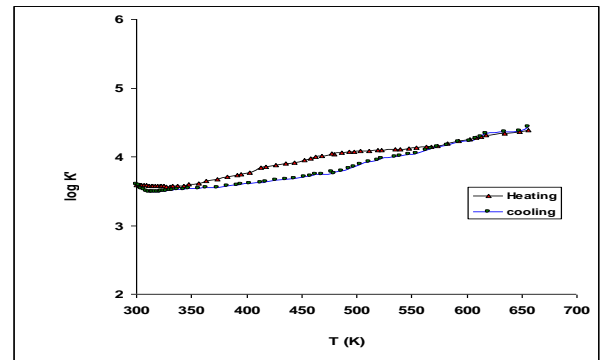


Figure-5. Plot of Dielectric Constant ($\log K'$) Vs temperature(T) for the sample[FTSR]

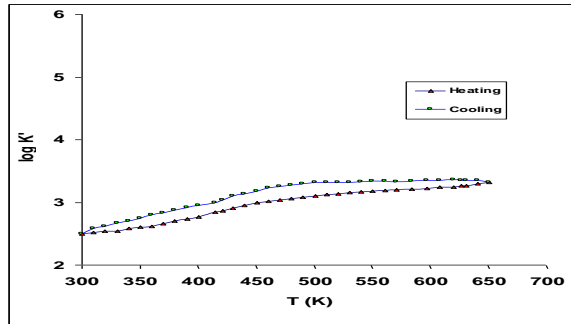


Figure-6. Plot of Dielectric Constant (logK') Vs temperature (T) for the sample [FTA]

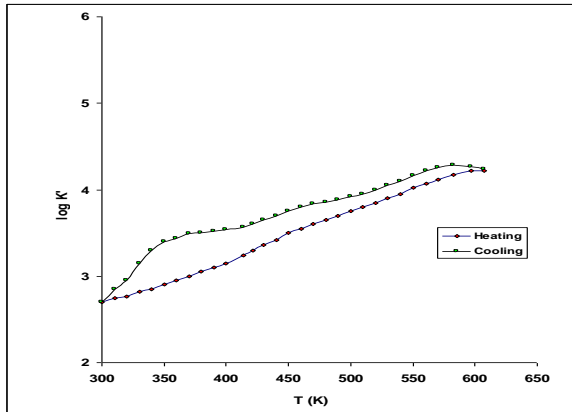


Figure-7. Plot of Dielectric Constant (logK') Vs temperature(T) for the sample[FTSA]

2.3 Electrical Properties:

The room temperature measurements of a. c. and d. c. resistivities along with the order parameter λ' , inhomogeneity and thermal ($\rho_{a.c.}$) hysteresis data are reported in the Table -2. The pseudobrookite is an n-type semiconductor [16]. Its conduction is associated with impurities, defects, interstices and therefore is complex. It is interesting to note that the a. c. resistivities increase by the use of anatase. Also the inhomogeneities are larger in the anatase based samples. Thus, the stress may be responsible to reduce the carrier density (space charge) and the mobility. The d. c. resistivities decrease in the anatase based pseudobrookites. Since the ($\rho_{d.c.}$) depends on the grain boundary, perhaps the increased porosity of anatase based samples decreases ($\rho_{d.c.}$) of these samples. The increase in order parameter λ' (i. e. the increase in lower tetrahedral symmetry at M2 site) appears to increase the a. c. conductivity.

Table -2: The electrical measurements at Room temperature

Sample	Inhomogeneity	Order Parameter λ'	$\rho_{a.c.}$ (ohm-cm)	$\rho_{d.c.}$ (ohm-cm)	Loop area of $\rho_{a.c.}$ hysteresis (Sq. Units)	Transition temp. T (K)		Activation Energy (eV)			Band gap (eV)
						T ₁	T ₂	Ea ₁ (350-440)	Ea ₂ (440-560)	Ea ₃ (560-850)	
[FTR]	-0.0020	0.310	6565	5.5	1.17	400	710	0.14	0.38	0.73	0.76
[FTSR]	-0.0025	1.000	9293	5.5	3.55	440	645	0.13	0.58	0.45	1.16
[FTA]	-0.0038	0.040	1040	849	17.00	390	710	0.22	0.45	0.80	0.90
[FTSA]	-0.0030	0.060	252	107	1.52	400	585	0.08	0.54	0.26	1.08

2.3.1 Variation of a.c. resistivity (1 kHz) with temperature:

The dependence of a. c. (1 kHz) resistivity ($\rho_{a.c.}$) on temperature is investigated from 300 to 850 K. The graphs of the log (ρ) versus the reciprocal of absolute temperature (1/T) of the samples [FTR], [FTSR], [FTA] and [FTSA] under study are depicted in Figures-8 to 11 respectively. The curves corresponding to heating and cooling are depicted in these figures to facilitate the investigation of 'Thermal Hysteresis' due to microcracking observed in the pseudobrookite [17]. Which affects the thermal conductivity and therefore also the electrical conductivity.

The curves show two transition temperatures T₁ (390-440 K) attributed to extrinsic-intrinsic transition and T₂ (560-710 K) attributed to antiferro to paramagnetic transition [20] and hence three distinct activation energies are observed and are shown (Table-2) as (Ea₁), (Ea₂) and (Ea₃) corresponding to the temperature regions (i) 350-440 K, (ii) 440-560 K and (iii) 560 – 850 K respectively. A short region commences with a positive temperature coefficient (PTC) except for samples [FTR] and [FTSA]. Which is followed by a region of small activation energy (Ea₁ ≈ 0.1 eV). This activation energy agrees with the reported value [16], where magnitude of mobility is small corresponding to small polaron and mobility increases with temperature. Therefore, the conduction in this region is attributed to small polaron hopping in extrinsic region and extrinsic-intrinsic transition takes place at around 440 K. The activation energy (Ea₂ ≈ 0.4 to 0.7 eV) of the second region is observed to be larger than that of the first region.

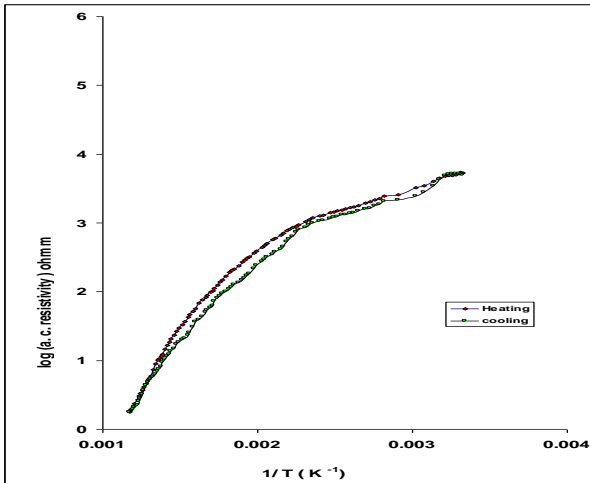


Figure-8. Plot of A.C. Resistivity Vs Reciprocal of temperature (1/T) for the sample[FTR]

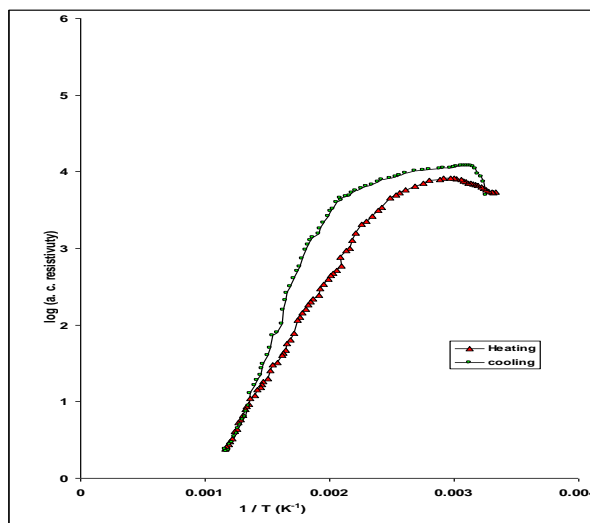


Figure-9. Plot of A.C. Resistivity Vs Reciprocal of temperature (1/T) for the sample[FTSR]

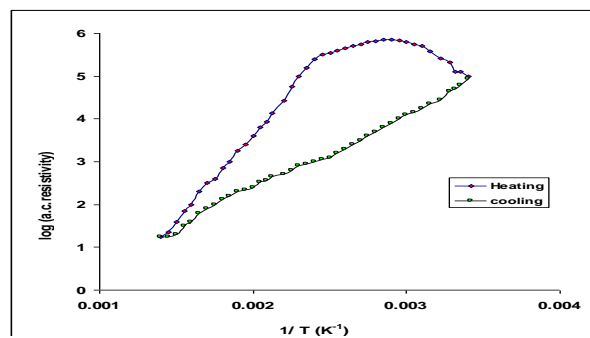


Figure-10. Plot of A.C. Resistivity Vs Reciprocal of temperature (1/T) for the sample[FTA]

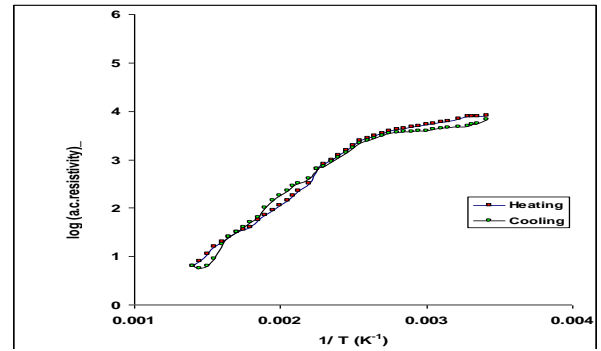


Figure-11. Plot of A.C. Resistivity Vs Reciprocal of temperature (1/T) for the sample[FTSA]

The conduction in this region is attributed to be due to the large polarons in the intrinsic region. $2 E_{a2}$ is, therefore, regarded as the band gap which ranges from 0.8 to 1.2 eV. The band gap is larger for the anatase based pseudobrookite. The transition temperature (T) is attributed to the antiferro-paramagnetic transition. The third region from 560 to 850 K is therefore called post transition region and the activation energy ($E_{a3} \approx 0.25$ to 0.75 eV) for this region is tabulated in the Table-2. It is interesting to note that the loop area of (ρ_{ac}) hysteresis increases with order parameter λ' in case of rutile samples whereas it decreases in case of anatase samples. It is also interesting to note that the samples [FTSR] and [FTSA] exhibit antihystereses and $E_{a3} < E_{a2}$ for these samples (Table -2). Hence we may conclude that these antihystereses are due to tunneling effect [21].

3. CONCLUSIONS:

It is interesting to note that substitution of Ti^{4+} by Sn^{4+} is responsible to increase the unit cell volume and X-Ray or theoretical density. On the other hand, the use of anatase in the reaction causes the decrease in practical density and the increase in the porosity, Debye particle size and the inhomogeneity. This may be attributed to the vertex –sharing network of anatase which is opposite to the edge – sharing network of the pseudobrookite. However, tin has exactly opposite effect on the anatase as the practical density, porosity, inhomogeneity and the Debye particle size are concern. It is observed from the dielectric measurements that the anatase causes the reduction in the space charge. If $K'_{1000\text{ kHz}}$ represents the contribution to the dipolar polarization, then interestingly the anatase enhances the dipolar polarization considerably. On the other hand, the presence of Sn^{4+} increases the contribution towards both the space charge as well as dipolar polarization. However, the increase in the space charge is significant.

The hysteresis of space charge decreases in area whereas hysteresis of dipolar polarization increases in area with the increase in order parameter λ' . The post transition activation energies (E_{a3}) and the transition temperatures (T) decrease with order

parameter λ' in case of anatase as well as rutile samples. It is also interesting to note that the samples [FTSR] and [FTSA] exhibit antihystereses and $E_{a3} < E_{a2}$ for these samples. Hence we may conclude that these antihystereses are due to tunneling effect.

REFERENCES:

- 1) D. A. Khramov, M. A. Glazkova, S.S. Meshalkin (1995). *J. Magn. Mag. Materials*, 150, pp. 101.
- 2) S. S. Meshalkin, M. A. Glazkova, D. A. Kharmov, V. S. Urusov (1994). *Mater. Sci. Forum*, 166-169, pp. 717.
- 3) G. M. Irwin, E. R. Sanford (1991). *Physical Review B*, 44, 9, pp. 4423-4430.
- 4) S. V. Salvi, A. H. Karande, M. A. Madare, S. S. Gurav (2005). *J. Ferro. and Inte. Ferro., Netherland*, 323, pp. 97.
- 5) L. V. Deshpande, V. G. Bhide (1960). *Lett. Alla Redazione*, pp. 816.
- 6) X. Z. Ding, Z. A. Qi, Y. Z. He (1994). *J. Nano Stru. Mater.*, 4, 6, pp. 663.
- 7) S. Mahanty, S. Roy, Suchitra Sen (2004). *J. Crys. Growth*, 261, pp. 77.
- 8) V. Ravi, S. K. Date (2001). *Bulle. Mater. Sci.*, 24, 5, pp. 483.
- 9) Noel Nava, Thomas Viveros (1999). *Hyperfine Inter.* 122, pp. 147.
- 10) C. H. Bartholomew, M. Budart (1973). *J. Catalysis*, 29, pp. 278.
- 11) William W. Coffeen (1953). *J. Amer. Cer. Soc.*, 36, 7, pp. 207.
- 12) Frank J. Berry, O. Helgason (2000). *Hyper. Inter.*, 126, pp. 269.
- 13) F. J. Berry, C. Greaves, J. McManus, M. Mortimer (1997). *G. Oates, J. Sol. Stat. Chem.* 130, pp. 272.
- 14) S. R. Dhage, V. Ravi, S. K. Date (2003). *Bull. Mater. Sci.* 26, 2, pp. 215.
- 15) Linus Pauling, *Nature of Chemical Bonds*, 3rd Edn. Cornell Univ. Press, Ithac., New York.
- 16) R. S. Singh, T. H. Ansari, R. A. Singh, B. M. Wanklyn, B. E. Watt (1995). *Sol. Stat. Comm.*, 94, 12, pp. 103.
- 17) H. J. Siebeneck, O. P. H. Hasselmann, C. J. Cleveland, R. C. Bradt (1976). *J. Am. Ceram. Soc.* May-June, pp. 241.
- 18) T. Birchall, N. N. Greenwood and A. F. Reid (1969). *J. Chem. Soc. A* pp. 2388.
- 19) P. T. Supe and K. R. Rao (1974). *Current Science*, 43, pp. 377.
- 20) U. Atzmony, G. Gorodetsky, E. Gurewitz (1979). *Phys. Rev. Lett.* 43, 11, pp. 782.
- 21) S. Gueron, M. M. Deshmukh, E. B. Myers and D. C. Ralph (1999). *Phys. Rev. Lett.*, 83(11), pp. 4148.

Corresponding Author

Dr. Sandesh S. Gurav*

Department of Physics, K. E S. Anandibai Pradhan Science College, Nagothane, Maharashtra